THE INFLUENCE OF CONTACT GEOMETRY AND SUB-CONTACT PASSIVATION ON THE PERFORMANCE OF SCREEN-PRINTED AL₂O₃ PASSIVATED SOLAR CELLS

Thomas Lauermann, Annika Zuschlag, Sascha Scholz, Giso Hahn, Barbara Terheiden
University of Konstanz, Department of Physics, 78457 Konstanz, Germany

Author for correspondence: Thomas.Lauermann@uni-konstanz.de, Tel.: +49 7531 88 2082, Fax: +49 7531 88 3895

ABSTRACT: This paper evaluates possibilities to passivate the semiconductor-metal interface present at the contact sites of large-area PERC-type solar cells to minimize recombination losses at the rear side. It focuses on the contact and BSF formation by local alloying of screen printed Al in a belt furnace process and methods to limit the detrimental lateral Si transport away from the contact sites.
The influence of different contact geometries and the resulting local BSF formation on the IV performance on cell level is assessed. For this purpose, 125×125 mm^2 p-type Cz-Si solar cells are processed with a screen printing based solar cell process where Al$_2$O$_3$ is used as rear side dielectric and a variety of rear contacting patterns is implemented.
Keywords: Passivation, Back-Surface-Field, Aluminum Oxide

1 INTRODUCTION

The superior passivation properties of Al$_2$O$_3$ for p-type silicon, the most common solar cell base material, are widely acknowledged [1,2], and respectable performances on lab cells [3] as well as industrial cells [4], [5] were demonstrated. Recently, several industrially applicable ways of using Al paste and firing to establish contacts to an Al$_2$O$_3$-passivated base were reported: Firing fritless paste on a pre-opened layer [4], investigations on pre-opened finger-like structures [6] or firing fritted paste in an H-pattern directly through the layer [7].

This paper focuses on the properties of the contact and BSF (Back Surface Field) formation by locally alloying Al paste in a belt furnace process and the challenges specific to it. In particular the formation of caverns at contact sites that complicate BSF epitaxy are highlighted. These cavities are the result of the lateral Si transport away from the contact sites by means of diffusion as published by Meemongkolkiat et al. [8]. To limit this effect and to achieve local SRVs (Surface Recombination Velocities) below 1000 cm/s by an optimized p$^+$ region, two different geometries and two new patterned screen printing approaches are investigated by measuring the resulting BSF thickness and homogeneity with the SEM (Scanning Electron Microscope). The contact performance on cell level is assessed by comparing IV data of Si solar cells made on 125×125 mm^2 Cz (Czochralski)-Si wafers.

2 MOTIVATION

As the quality of the passivation layers rises, the passivation of the contacts becomes increasingly important regarding the cell efficiency. This can be deduced from the equation derived by Fischer [9], stating that the effective SRV S$_{eff}$ is composed of the SRV of the passivated area S$_{pass}$ and the SRV of the metalized fraction S$_{met}$ in the following way:

$$S_{eff} = \frac{D}{W}\left[\frac{p}{2W\sqrt{\pi f}}\,arctan\,\frac{2W}{p}\sqrt{\frac{\pi}{f}} - e^{-\frac{W}{p}} + \frac{D}{fWS_{met}}\right]^{-1} + \frac{S_{pass}}{1-f} \quad (1)$$

Here, W is the wafer thickness, D is the diffusion constant, p is the contact pitch and f is the metalized

fraction. In Fig. 1 it can be seen that solar cells do not improve significantly from advancements made in the field of dielectric passivation below 20 cm/s if unpassivated contacts (red lines) are used. In this calculation, a metallization fraction of 7% and 1 mm pitch was assumed.
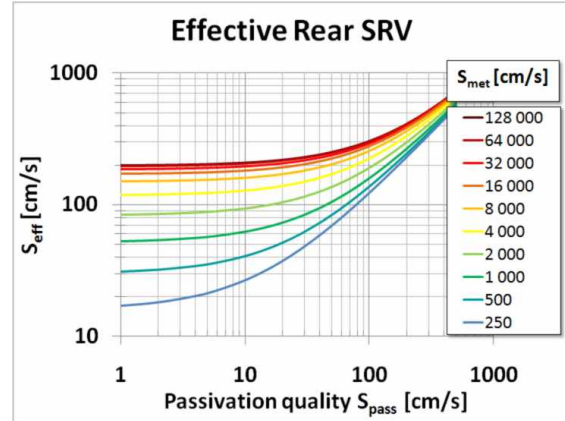

Figure 1: Graphic representation of Fischer's equation for a variety of contact recombination velocities (S$_{met}$, given by the color code).

It is obvious that when using a state of the art Al$_2$O$_3$ passivation with S$_{pass}$ < 5 cm/s [2], the metallization is the limiting factor for the rear side and S$_{eff}$ can be reduced to less than one fifth when using passivated contacts with S$_{met}$ <500 cm/s (turquoise line), compared to the case in which unpassivated contacts are used.

Therefore, our work focuses on achieving a thick, highly and homogeneously doped BSF directly beneath the contacts by locally alloying aluminum paste into silicon during the co-firing process.

3 THEORY OF LOCAL CONTACT FORMATION

The principles of homogeneous BSF formation from the application of screen-printed Al paste is well understood [10]. During the heating ramp of the firing process, the Al melts and dissolves more and more Si as temperature rises, corresponding to its solubility at a given temperature [11]. At peak temperature, a hypereutectic liquid alloy with Si contents well above

25% depending on the temperature is present in the paste matrix as well as on the wafer surface. During the cooling ramp the liquid alloy ejects Si from the melt when its Si concentration is above the maximum solubility at a given temperature, forming the heavily Al-doped layer known as BSF.

When considering the local contacts of PERC (Passivated Emitter and Rear Cell) [12] solar cells, the situation gets more complicated. Now the local Si concentration in the alloy during a given point in time during firing depends also on the distance to the nearest contact region, since only the pre-opened contact sites contribute to Si saturation in the paste. The concentration gradient between the high Si concentration above the contact sites and the Si-free Al melt everywhere else drives a lateral diffusion of Si away from the Si/molten Al interface. A Gaussian distribution of Si in the alloy can be assumed at peak temperature [13], with the peak level of the Si concentration directly above the contact site which is lower than that of homogeneous BSF formation. This has two implications for the local BSF formation: First, a lower concentration means that epitaxy is starting at lower temperatures during the cool-down phase. Thus the Al dopant peak concentration is lowered. Second, a lower Si concentration above the eutectic composition means less Si is available for epitaxy and therefore the BSF thicknesses is smaller. Both effects affect the desired passivation quality of the contact sites adversely [14].
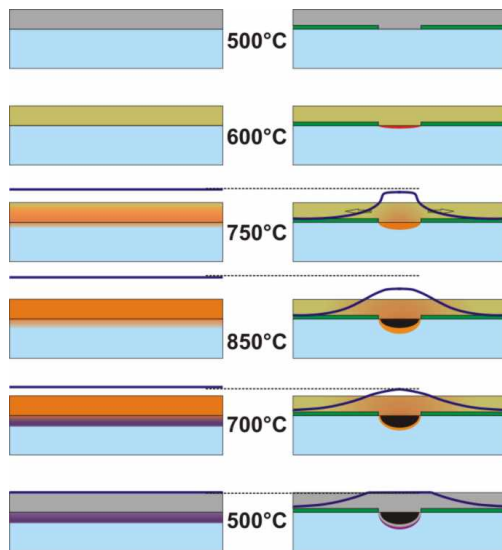

Figure 2: Schematic illustration of the homogeneous and the local alloying process with the blue solid line representing hypereutectic Si concentration as measured by [13] and the dashed line representing the solubility at a given temperature. In the local case, BSF formation starts later in the process, here at 700°C as opposed to 850°C for the homogeneous case.

Accordingly, it is desired to retain a sufficient amount of Si in hypereutectic concentration above the contacts during the cooling ramp. For this reason, methods to hinder the out-diffusion of Si are investigated in this work that include using line contacts instead of points to restrict diffusion to one direction and printing Al paste only on the desired contact site. This is done complementary to the research of other groups that investigate the addition of Si into the paste [15].

4 EXPERIMENTAL METHODOLOGY

4.1 SEM Samples

In the first part of our experiment, contact samples are prepared. This is done by depositing a 75 nm PECVD (Plasma-Enhanced Chemical Vapour Deposition) SiN_x layer on alkaline-etched Cz Si wafers. Subsequently, the structuring of the dielectric layer is carried out by printing a negative mask and opening the vias in aqueous HF solution with an industrial inkjet printer. After mask removal and cleaning, Al paste is applied by screen printing, either on the full area or locally matching the opened structure, depending on the design used.

The following designs are implemented:
- A: Point openings with varying contact size, fully covered with Al paste.
- B: Line openings with varying contact width, fully covered with Al paste.
- C: Point openings covered with Al paste dots matching the opened areas.
- D: Fritted Al paste dots on an uncapped, unstructured Al_2O_3 layer. Here, no SiN_x was used since it would aggravate the fire-through process.
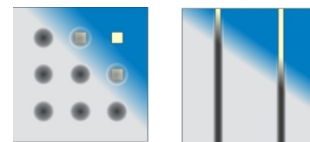

Figure 3: Schematics of the samples A and B receiving a fully covering Al paste layer. The grey Al paste is made semi-transparent to see the underlying passivation layer and the exposed silicon.
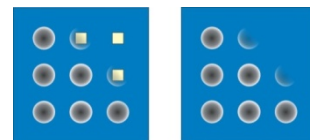

Figure 4: Schematics of the sample types C and D with partial application of Al paste.

The samples are cleaved along the crystal orientation and their cross section is investigated for cavern formation, BSF thickness and contact area between Si and Al-Si-alloy using SEM.

4.2 Performance evaluation on solar cell level

With the help of the SEM results, parameters are chosen for solar cell production. They are fabricated on 2 Ωcm 125×125 mm² Cz-Si wafers, using the industrial cell processing facilities at University of Konstanz, following the processing sequence previously developed in [4]. To minimize the influence of the emitter, whose recombinative properties usually dominate the V_{OC} of industrial solar cells, a selective emitter structure is chosen as described in [16]. In that case V_{OC} can be used as an indicator of rear surface passivation quality. 15 nm of Al_2O_3 are deposited as the primary rear side passivation using an Oxford ALD tool (Flex-AL) and subsequently capped by 75-160 nm of SiN_x deposited by remote-plasma PECVD. No additional annealing is performed on the cells, with only the co-firing step activating the passivating properties of the Al_2O_3.

Table I: Process flow chart for dielectrically passivated solar cells and full area BSF references. For group D, the structuring steps (*) are omitted.

References	Passivated Cells
Alkaline texture	
30 Ω/sq emitter diffusion	
	Emitter removal rear
	Rear Al$_2$O$_3$, SiN$_x$ deposition
Inkjet masking front	… and rear*
Sel. emitter formation	… and via etching*
PECVD SiN$_x$ ARC	
Screen printing Ag front grid and full Al rear side	
Co-firing	

Note that except for the first experiment with pattern A, different Al pastes were used for the references and the locally contacted cells. It was found that pastes with good local alloying behavior do not necessarily lead to the best results on full-area BSF cells. Therefore, the most suitable paste for each purpose was selected.

5 RESULTS

5.1 Point contacts, full area Al coverage

When considering point contacts with a full area Al back side as used with samples A, it is found that cavity formation occurs. The dissolved silicon follows a concentration gradient in the paste during the heating ramp of the firing process and gets transported away from the contact site (see Fig. 5). This Si is unable to contribute to BSF epitaxy, since it is too far away from the contact interface. On the other hand, the concentration of Si in the Al paste at the interface is too low to be expelled from the melt during cool down. This leads to an unpassivated contact, unless the point contacts exceed widths of around 200 µm, and special firing parameters as well as suitable pastes as published by [8] are used supporting local Si saturation. Under these circumstances, the contacts show a partial filling with Al-Si-alloy and BSF formation is observed (see Fig. 6), leading to a better overall performance on cell level (see Tab. II).
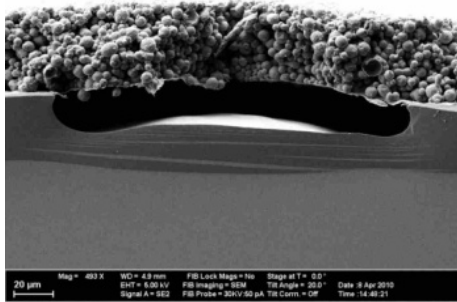

Figure 5: SEM Cross section of design A with 200 µm wide point contacts fired with standard firing parameters.
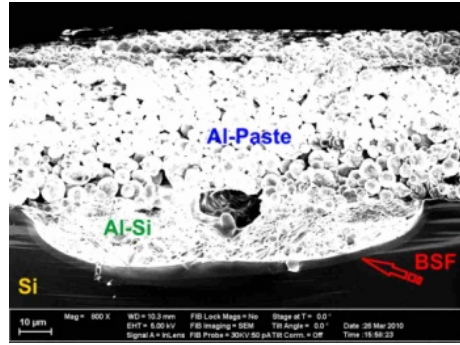

Figure 6: SEM Cross section of design A with 200 µm wide point contacts. Here firing parameters have been modified to enhance Si saturation.

Table II: IV results from the best solar cells with contact type A, previously published in [4].

	j$_{SC}$ [mA/cm²]	FF [%]	V$_{OC}$ [mV]	η [%]
References	36.4	79.5	619.1	17.9
Unpass. cont.	37.5	77.6	629.5	18.3
Pass. cont.	37.8	77.2	638.6	18.6

Depending on the alloying conditions, the BSF thicknesses vary from zero to 6 µm. This effect is mainly responsible for the observed V$_{OC}$ difference of about 9 mV. Note that the current densities of the references are lower than published for comparable selective emitter designs due to larger finger widths (same finger width for references and passivated contact cells) and a more conservative etch-back. The design is kept constant for all following experiments (shown in Table II-V) for the sake of comparability.

5.2 Line contacts, full Al coverage

When using line contacts in design B instead of point contacts, obtaining a solid Al-Si-alloy filled contact becomes much less sensitive to the firing conditions. BSF formation is generally observed with thicknesses of 4 µm to 7 µm. Here the lower limit for groove widths that reliably show full contact to a solid alloy ranges from 60 µm to 90 µm depending on paste and firing conditions. Narrower grooves, however, remain hollow.
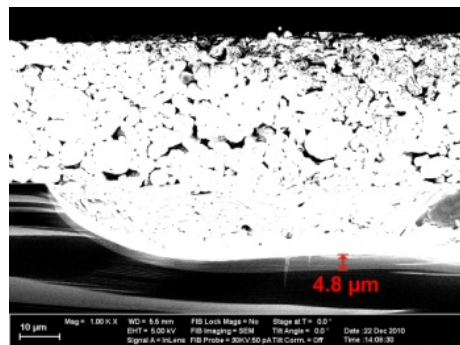

Figure 7: Contact type B, SEM cross section of a 90 µm wide line opening.

Table III: IV results from the best solar cells with contact type B. An improved Al Paste is used for the references compared to the cells in Tab. II, yielding better V_{OC}.

	j_{SC} [mA/cm²]	FF [%]	V_{OC} [mV]	η [%]
References	36.7	78.6	631.9	18.2
Passivated	37.7	78.3	640.0	18.9

Here, an improvement compared to group A can be seen in the higher V_{OC} as well as the better fill factor achieved by line contacts. This can be attributed to the increased probability of achieving a complete and solid contact between semiconductor and alloy enveloped by a thick BSF compared to the point contacts in group A.

5.3 Point contacts, partial Al coverage

No cavity formation is found in the SEM images of contact type C. The cross section shows a 6 µm thick BSF (red) that is, however, discontinuous (yellow) at some points (Fig. 9). Apparently, the amount of Al paste available for BSF formation is too low under these circumstances. To balance this, the vias were made somewhat smaller than the Al dots for the solar cell experiments.
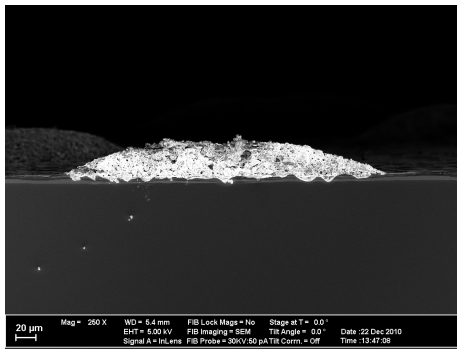

Figure 8: Contact type C, point contact printed over corresponding opening in dielectric.
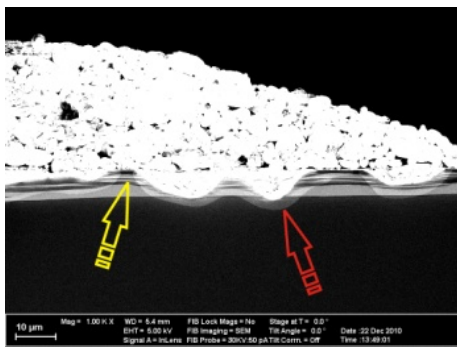

Figure 9: SEM close-up of contact type C, thick BSF visible (red) with discontinuities (yellow).

Table IV: IV results from some solar cells with contact type C. For IV measuring, the paste was etched off and 2 µm of Al was evaporated.

	j_{SC} [mA/cm²]	FF [%]	V_{OC} [mV]	η [%]
Best Ref.	36.0	78.7	632.2	17.9
Best Pass.	36.4	72.1	641.8	16.9
Remarkable	37.0	69.7	652.2	16.8

Unfortunately, measuring these cells as fired properly on a flat chuck is nearly impossible due to the height differences of the spots leading to the majority of the Al dots having no electrical contact to the chuck. This is resolved by etching off the Al paste and e-beam evaporation of a flat 2 µm Al layer. After 30 min of annealing at 380°C, a complete rear contact is established and the IV curve can be measured. Passivation and other solar cell properties remain unchanged during this treatment, since the V_{OC} values before and after evaporation show no significant difference.

The V_{OC} shows unusual deviation across the batch with the cell featuring the highest voltage achieving 652.2 mV. This indicates that while the contact passivation can be considered very good in general, since it leads to voltages above 640 mV, not all contacts are formed in the same way and optimal contact passivation is very sensitive to slight variations in the opening patterns and other environmental conditions during processing (see section 5.5). However, the fill factor suffers from additional series resistance. Using electroluminescence and the Corescan method, this could be traced back to elevated contact resistance of the Ag front grid. It can be assumed that the missing absorption and heat capacity of a fully covering Al layer on the rear side affected the wafer temperature during firing, causing insufficient front contact formation.

5.4 Partial Al coverage, fire-through process

The solar cells metalized with design D show only a slight increase in V_{OC}. This indicates that the passivation layer reduces rear side recombination, but its S_{eff} is limited to values of around 200 cm/s by lack of contact passivation (see Fig. 11). Optical microscopy results reveal an incomplete opening of the Al_2O_3 layer during firing and inhomogeneous contact formation. The measured solar cell series resistances exceed 5 Ωcm² which explains the low fill factors of around 50%.
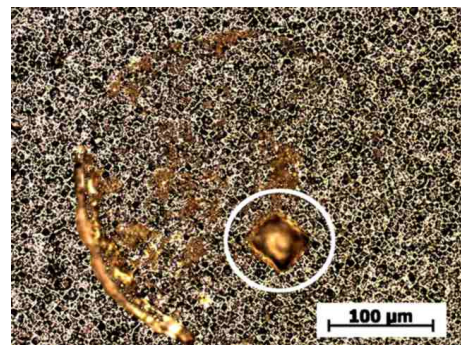

Figure 10: Contact type D, optical microscopy top view. Contact alloying is only observed at small fractions of the contact area (marked white).
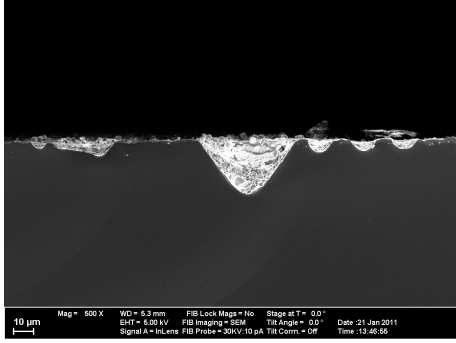
Figure 11: Contact type D, SEM cross section. A shallow BSF is barely visible under the sparsely distributed contact spots.

Table V: Results of solar cells metalized with design D. Unfortunately the j_{SC} is limited by improper anti-reflection coating.

	j_{SC} [mA/cm²]	FF [%]	V_{OC} [mV]	η [%]
References	35.9	78.6	636.4	17.9
Design D	36.6	51.1	638.7	11.9

To furthermore complicate the solar cell evaluation, the adhesion on pure Al_2O_3 of the pastes used in this study is very weak compared to adhesion on SiN_x. A substantial amount of contacts starts to peel off, leading to the electrical isolation of the affected vicinity. If a fire-through approach was to be developed, additional efforts should be directed into choosing suitable paste compositions as well as printing and drying conditions, which is beyond the scope of this work.

5.5 Comparison of contact passivation

Since the reference solar cells processed with each group showed slight differences, especially in V_{OC}, a direct comparison is difficult. Hence we take a look at the rear surface recombination by means of LBIC (Light Beam Induced Current), where a 980 nm laser is used to locally probe quantum efficiency and assess qualitatively the rear side recombination velocity of the contacts by using the passivated area as a baseline.
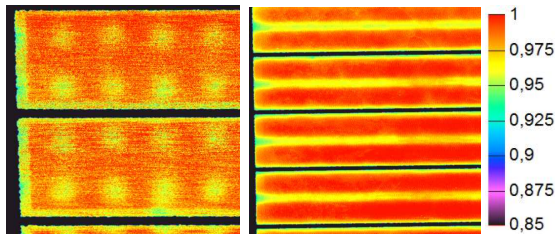

Figure 12: LBIC images @980nm of type A and B cells. The scaling of the measured short circuit current is relative to the Al_2O_3 background.

In Figure 12 on the left, the point contacts (200×200 μm² in size) of the best cell from group A are visible by the signal drop to about 95-96% of the j_{SC} value of the passivation layer. Minor deviations from point to point can be noticed. In the case of 90 μm lines, shown in the right picture, a homogeneous signal of 96% can be found all along the lines. Note that due to

overlaying with the front contact grid 50% of the contact area is "hidden" behind the front contact fingers.
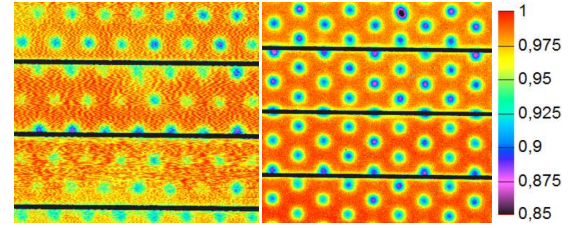

Figure 13: LBIC images @980 nm of solar cells from type C on the left and type D on the right. The scaling of the measured short circuit current is relative to the Al_2O_3 background.

In Figure 13 for the group C solar cells pronounced differences in the contact passivation can be seen not only from cell to cell, but even on neighboring contacts ranging from near-perfect passivation around 97% to values down to 90% (left). The contacts of the solar cells from batch D (right) go well below 90%, indicating lack of passivation.

Taking a closer look at the different contacts of group C, it can be seen that the different contact quality relates to the completeness of the surface alloying. The Si dissolution process starts locally, expands over the contact surface and leads only to a complete area coverage if enough Al is available. Otherwise, unalloyed, unpassivated structures can be seen beneath the contacts after etching them off in HCl (Fig. 14).
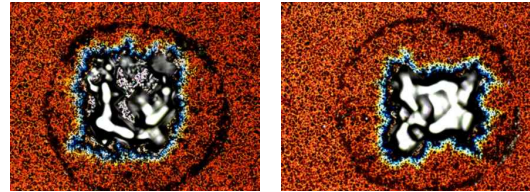

Figure 14: An etched-off contact (180 μm) revealing incomplete BSF alloying at the island-like structures (left) and a slightly smaller contact (160 μm, right), completely alloyed.

This behavior was described by Huster in [10] and relates directly to the applied amount of paste. Therefore, we can conclude that a careful fine tuning of the paste spot thickness, area and overlap is necessary to achieve a homogeneous contact quality across the solar cell. Optimized point contacts, however, show the thickest BSF and consequently the highest voltages and quantum efficiencies on cell level.

6   DISCUSSION

The formation of cavities occurs when the paste above the contact is not sufficiently oversaturated with silicon during the cooling ramp. Under these circumstances, no or very shallow BSF formation in the range of below 2 μm is observed, leading to unpassivated contacts with S_{met} in the range of 10^5 cm/s as discussed in [4]. The transport of dissolved silicon into the paste away from the contact interface with Si is the main reason for this effect.

Adapting the firing parameters and using sufficiently large areas for the vias can help to overcome this problem. However, the results suggest that reducing the dimensionality of the transport directions is a more promising approach.

With design B, this gradient-driven transport phenomenon occurs in only one direction. Therefore, the lines can be kept very narrow, since according to [6] the contact resistance does not improve significantly with a larger line width and the formed grooves are alloy-filled down to 60 µm width. This also translates into higher efficiency, because V_{OC} shows a general improvement despite the slightly higher metallization fraction (8% for B compared to 6% for A) on the rear side. It also affects the fill factor beneficially even though the average transport length of the photogenerated majorities is slightly larger for design B (292 µm) than for design A (276 µm). This behavior could be explained by less current crowding at line contacts compared to point contacts.

With design C, where there are no transport directions for silicon, no cavity formation is detected. Directly under the alloy, a thick BSF is formed. However, the BSF is not uniform over the whole contact metalized area, indicating an oversaturation of the sparsely applied Al paste. Applying a larger amount of paste and printing paste on an area slightly wider than the opening width to offer more Al during alloying was chosen for solar cell production as a compromise between oversaturation in this case and the undersaturation observed with samples A and B. It is found that the sweet spot for optimal contact passivation seems to be quite small, so careful tuning of the applied Al amount to the opened area is required, otherwise inhomogeneous BSF formation is observed resulting in a large spread of V_{OC} values. Furthermore, such a rear side concept is difficult to contact, since the current has to be collected from the individual contact spots. Also, the firing temperatures and peak dwell times have to be adjusted to account for the missing metal on the rear side. If these issues are addressed though, the resulting solar cells show the best V_{OC} and the highest local IQE in the long-wavelength spectrum in comparison to the other rear contacting methods.

It is, however, recommended to open the desired contact spots before printing and firing, as we could not achieve uniform low-ohmic alloyed and passivated contacts by etching through the dielectric layer using fritted paste. This is demonstrated with the solar cells with contact type D.

7 SUMMARY

In this paper, the possibilities of achieving improved contact passivation for large area screen printed PERC-type solar cells using Al_2O_3 as passivation for the p-type base on the rear side are discussed. It is demonstrated that contact passivation is important since it becomes the limiting factor when using passivation layers with low recombination velocities. This passivation is achieved here by locally alloying screen-printed Al paste into the Si, forming a BSF at the contact sites.

The challenges when using local contacts are discussed, which are diffusion of Si away from the contact sites, leaving unpassivated voids in the bulk. This can be compensated by adapting the firing parameters, by

restricting the diffusion directions to one dimension when using lines or inhibiting it altogether by printing the paste itself only locally. The latter proves to be challenging, so that the best cell results of 18.9% could be realized with a line contact pattern, achieving 640 mV in V_{OC}. This contact pattern shows a better contact passivation homogeneity across a solar cell in LBIC than the previously used point contacts and was also used independently by another group on their latest record efficiencies [5]. However, the best passivated rear contacts are observed on cells with local paste application on pre-opened contact spots, showing a V_{OC} of 652 mV and the highest LBIC readings. Therefore, the potential of this contacting method justifies further attention, though some work still needs to be done in optimizing paste overlap and their firing behavior.

8 REFERENCES

[1] B. Hoex, S.B.S. Heil, E. Langereis, M.C.M. van de Sanden, W.M.M. Kessels, Appl. Phys. Lett. 89 (2006), 042112

[2] G. Dingemans, W.M.M. Kessels, Proc. 5th WCPEC, Valencia, 2010, pp. 1083-1090.

[3] J. Schmidt, A. Merkle, R. Brendel, B. Hoex, M.C.M. van de Sanden, W.M.M. Kessels, Prog. Photovolt: Res. Appl. 16 (2008) 461.

[4] T. Lauermann, T. Lüder, S. Scholz, G. Hahn, B. Terheiden, Proc. 35th IEEE PVSC, Honolulu, 2010, pp. 28-32

[5] S. Gatz, H. Hannebauer, R. Hesse, F. Werner, A. Schmidt, T. Dullweber, J. Schmidt, K. Bothe, R. Brendel, Phys. Stat. Sol. RRL 5(4) (2011) 147.

[6] E. Urrejola, K. Peter, H. Plagwitz, G. Schubert, J. Appl. Phys. 107 (2010) 124516.

[7] I. Romijn, A.A. Mewe, E. Kossen, I. Cesar, E.E. Bende, M. N. van den Donker, P. van Eijk, E. Granneman, P. Vermont, A.W. Weeber, Proc. 5th WCPEC, Valencia, 2010, pp. 1432-1437.

[8] V. Meemongkolkiat, K. Nakayashiki, D.S. Kim, S. Kim, A. Shaikh, A. Kuebelbeck, W. Stockum, A. Rohatgi, Proc. 4th WCPEC, Hawaii 2006, pp. 1138-1141.

[9] B. Fischer, Loss analysis of crystalline silicon solar cells using photoconductance and quantum efficiency measurements, Ph.D. thesis, University of Konstanz, 2003.

[10] F. Huster, Proc. 20th EU PVSEC, Barcelona, 2005, pp. 1466-1469.

[11] J.L. Murray, A.J. McAlister, The Al-Si system, Bulletin of alloy phase diagrams 5(1) (1984).

[12] A.W. Blakers, A. Wang, A.M. Milne, J. Zhao,

M.A. Green, Appl. Phys. Lett. 55(13) (1989) 1363.

[13] E. Urrejola, K. Peter, H. Plagwitz and G. Schubert, Appl. Phys. Lett. 98 (2011), 153508

[14] M.P. Godlewski, C.R. Baraona and H.W. Brandhorst, Proc. 10th IEEE PVSC, Palo Alto, 1973, pp. 40–49.

[15] M. Rauer, R. Woehl, C. Schmiga, M. Hermle, M. Hörteis, D. Biro, IEEE Electron Device Letters 32(7) (2011) 916.

[16] T. Lauermann A. Dastgheib-Shirazi, F. Book, B. Raabe, G. Hahn, H. Haverkamp, D. Habermann, C. Demberger, C. Schmid, Proc. 24th EU PVSEC, Hamburg, 2009, pp. 1767-1770.